Design criteria assessment of a magnetic nozzle

Physica Scripta

PAPER

Design criteria assessment of a magnetic nozzle

Yung-An Chan[1] and Georg Herdrich[2]

[1] Institute of Aerodynamics and Flow Technology, German Aerospace Center, Göttingen, Germany
[2] Institute of Space Systems, University of Stuttgart, Stuttgart, Germany

E-mail: yung-an.chan@dlr.de

Keywords: magnetic nozzle, MHD, neutralizer-free, electric propulsion

OPEN ACCESS

RECEIVED
19 October 2023

REVISED
11 December 2023

ACCEPTED FOR PUBLICATION
14 December 2023

PUBLISHED
28 December 2023

Abstract

A model to assess the design criteria for a convergent-divergent magnetic nozzle is provided. This model is based on an ideal single-fluid magnetohydrodynamic flow assumption to evaluate the acceleration and detachment in the magnetic nozzle. A thermodynamic correlation of plasma internal energy during the propagation in a magnetic nozzle is presented. The result reveals the limitation of a magnetic nozzle on the conversion of internal energy to kinetic energy, where an upper limit of around 19% is derived, assuming plasma undergoes ideal conditions. In addition, criteria derived from the model also point out that a threshold on magnetic flux density exists to prevent the occurrence of flow discontinuity during propagation along the magnetic nozzle. The result hints at the essential role of the electric field on the acceleration processes of a magnetic nozzle, which can potentially be the key to overcoming the limitation of a magnetic nozzle's performance.

1. Introduction

The magnetic nozzle (MN) is a device used for providing constraint to plasma and converting the internal energy of plasma into kinetic energy. It is commonly used in electric propulsion, especially with neutralizer-free thrusters [1, 2], such as helicon plasma sources [3–6], electron-cyclotron-resonance sources [7–10], Magnetoplasmadynamic thrusters [11], or vacuum cathode arc thrusters [12].

The most straightforward MN concept can be achieved by applying DC flow on a conductive loop wire, which generates magnetic dipole in a rotational-symmetry configuration, as figure 1 shows. On the one hand, the Lorentz force applied on the charged particles can constrain plasma flow within the dipole, which inhibits particle transportation across the streamline of magnetic flux, providing plasma confinement and preserving the kinetic energy of the charged particles from losing to the physical boundary. The electron is heated up by the electromagnetic wave sent from the high-frequency antenna.

The high-energy electrons form a diamagnetic current gyrating in the azimuthal direction of the static magnetic field. From a global perspective, the high-energy electrons act like energy carriers, and their kinetic energy is preserved in the diamagnetic current of plasma by the magnetic field constraint from MN. The MN converts the gyrokinetic energy of plasma into the kinetic energy parallel to the axis of the MN via Lorentz force and an ambipolar electric field [3]. The MN received a net momentum gain as long as the plasma detached from the magnetic dipole. The force imparted from the Lorentz force has been proven dominant in the global thrust generated by a helicon plasma thruster [13].

Two perspectives can explain the plasma acceleration mechanisms in MN: the ambipolar acceleration generated by the current-free double layer (CFDL) and the Lorentz force raised from the MHD theory. The CFDL has been identified by Charles and Boswell [14], where a potential drop near the exit of the MN provides ambipolar acceleration to the plasma. A similar result was also demonstrated by the particle-in-cell simulation. by Meige *et al* [15] and later by Rao and Singh in 2D [16]. Liebermann [17] further discovered that the potential drop is linearly correlated to the plasma source's electron temperature.

The MHD theory discusses an MHD flow's momentum and thermal energy conservation. The diamagnetic current of plasma in the MN is converted into the kinetic energy of charged particles according to the invariance

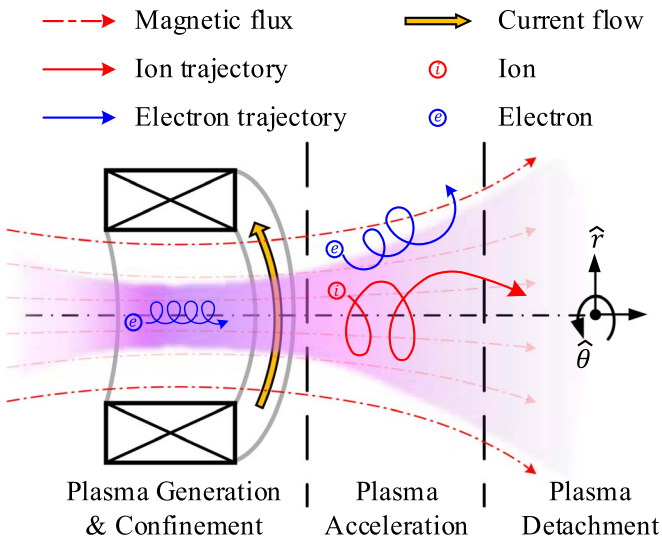

Figure 1. Concept illustration of the magnetic nozzle and the functionality of each section.

of the magnetic moment, where the transversal velocity of the charged particle is converted into the velocity along the magnetic flux vector [18, 19]. Experiments also demonstrated the contribution of diamagnetic current in the MN to the momentum gain of the thruster [13]. In addition, the appearance of the radial electric potential gradience due to the non-uniform distribution of charged particles in MN also imparts in the plasma acceleration processes through the $E \times B$ drift. Depending on the vector of E field, the $E \times B$ drift can provide either constructive or destructive effects on the plasma acceleration processes in MN [20].

In addition to plasma acceleration, numerous theories have been proposed for the plasma detachment in MN since the 1990s, which could be generally categorized into four directions [21]: Collisions and resistive detachment [22], Finite Larmor radius (FLR) [23, 24], Magnetic field perturbation [25, 26], and instabilities [27]. The FLR and the magnetic stretch theory are the most commonly used theory in MN. On the one hand, the FLR theory presented in [24] provides an insightful simulation of the detachment effect for the collisionless plasma, demonstrating the impact of the electron inertia. On the other hand, Takahashi and Ando measured the stretching B-field of a 2D time-resolved B-field with an inductive probe [28]. Desipte there has been wide discussions on the dominating effect, the actual driving mechanism has not yet been pinned down. Nevertheless, Deline *et al* [29] experimentally observed that plasma detachment occurred where plasma velocity succeeds the Alfvén velocity, also known as super-Alfvénic conditions, under different injecting conditions into MN. The results provide a useful boundary condition for plasma detachment assessment from electromagnetic influence.

The recent advancement of electronic thermodynamics in the MN, focusing on discussing the polytropic index (γ), has significantly improved the understanding of its plasma acceleration and detachment mechanism. Early experiments have demonstrated a nearly isothermal expansion of the plume ($\gamma \sim 1$ to 1.2) using a helicon plasma source with an MN [30–34]. Zhang *et al* [32] demonstrate that γ is strongly affected by the shape of electron energy participation function (EEPF), which is influenced by the non-local ambipolar effect from the CFDL. Takahashi *et al* [35] observe that the depletion of the high energy region of the EEPF is strongly correlated to the presence of an electric field along the axial position of the MN, suggesting that the CFDL trapped electrons is the cause of the isothermal condition.

The observation of the γ_e approaching/greater the adiabatic expansion processes ($\gamma_e = 1.67$) has been experimentally determined by Kim [36] and Vinci [37]. The experiment from Kim proposes a hypothesis that the presence of the radial electric field and axial magnetic flux would limit the electron's motion and reduce the degree of freedom of gaseous from 3 to 2, which allows the $\gamma_e = 2$ condition sustained in adiabatic expansion condition [36]. The similar γ_e values are also observed in Vinci's measurements [37], yet he attributes the unusual γ_e value to the non-linear effect or anisotropies processes, such as the present of multiple EEPF populations and instabilities. Nevertheless, the research of the γ_e provides a consolidate scope for engineering the MN.

Though MN is a simple engineering approach to provide plasma confinement and acceleration, the interpretation of plasma dynamics in MN is still relatively complex. Apart from this, most of the work about MN is based on experimental observation and/or oversimplified assumptions. So, how to design MN for space applications at a glance remains unclear or inconclusive. Unfortunately, too many parameters are involved and

intertwined with the tested conditions and the working principle of the different sources. It is unrealistic to comprehensively discuss the impact of individual design parameters from the source and working conditions.

This work aims to provide an analytical solution for a criteria assessment and a guideline for MN design based on the most straightforward MN configuration, i.e., a convergent-divergent MN. The work is based on single-fluid MHD assumptions and considerations to interpret the plasma phenomenon in MN. The theoretical assessment considered the effect of the plasma acceleration from convergent to divergent MN and the detachment criteria in MN. At the end of this work, design criteria for MN will be presented based on the assessment of the analytical model.

2. Fundaments of MHD flow

2.1. Momentum equation for Single-fluid MHD flow

Starting from the momentum equation for charged particles under the acting forces is written in equation (1):

$$\rho_m \frac{D\mathbf{v}}{Dt} = \rho_m \left(\frac{\partial \mathbf{v}}{\partial t} + (\mathbf{v} \cdot \boldsymbol{\nabla}\ )\mathbf{v} \right) = \rho_q \boldsymbol{E} + \boldsymbol{j} \times \boldsymbol{B} - \nabla\ p \tag{1}$$

[

This equation is from the MHD book, [38]. The left-hand side describes the time-dependent momentum variation of the flow, while the right-hand side of the equation describes the force applied to the MHD flow, which is (from left to right) electrostatic acceleration ($\rho_q \boldsymbol{E}$), electromagnetic acceleration ($\boldsymbol{j} \times \boldsymbol{B}$), and the pressure gradient (∇p). The ρ_q described the mean charged density of the local plasma flow; while ρ_m represents the local mean mass density of the plasma flow.

Under the assumption of the ideal MHD flow without an electric field, one can comprehend that increasing the kinetic energy of plasma flow could be achieved through increasing electromagnetic force $\boldsymbol{j} \times \boldsymbol{B}$ and the pressure gradient ∇p, respectively. Thus, optimizing the value of $\boldsymbol{j_e} \times \boldsymbol{B}$ and ∇p_e can lead to an MN performance optimization.

2.2. Pressure invariant characteristics

$$\nabla p = \boldsymbol{j} \times \boldsymbol{B} = \frac{1}{\mu_0}(\boldsymbol{\nabla} \times \boldsymbol{B}) \times \boldsymbol{B} = \frac{1}{\mu_0}\left[(\boldsymbol{B} \cdot \boldsymbol{\nabla})\boldsymbol{B} - \frac{1}{2}\nabla^2\ \boldsymbol{B} \right] \tag{2}$$

Rearranging equation (2) and introducing Gauss's law for Magnetism ($\nabla \cdot B = 0$), a correlation between pressure and applied B-field can be derived, known as pressure invariant in MHD flow, see equation (3).

$$\nabla\left(p + \frac{B^2}{2\mu_0} \right) = \frac{1}{\mu_0}(\boldsymbol{B} \cdot \boldsymbol{\nabla})\boldsymbol{B} = 0 \tag{3}$$

Here, the term $B^2/2\mu_0$ is known as magnetic pressure (p_m). This equation shows that the sum of gas-dynamic pressure (p) and magnetic pressure (p_m) is invariant in static equilibria plasma. From the physical perspective, the internal energy of the plasma system can be preserved in the B-field (as diamagnetic current) considering no external effect or loss presented in the plasma flow. The ratio of the gas-dynamic pressure and magnetic pressure leads to a dimensionless parameter β; see equation (4).

$$\beta = \frac{p}{p_\mathrm{m}} = {nk_\mathrm{B}T}\Big/{B^2/2\mu_0} \tag{4}$$

[

This parameter can represent the magnetization degree of the plasma fluid. When $\beta \ll 1$, the diamagnetic effect in the plasma is small, and the local B-field in the plasma is almost equal to the applied B-field B_0. When $\beta \approx 1$, the diamagnetic current counteracts the applied B-field, suggesting no applied B-field diffuses into the plasma. If $\beta > 1$, the plasma flow cannot be entirely confined by the applied B-field. For most MN used for EP devices, it is valid to assume that the plasma gas-dynamics pressure is dominated by the electron temperature (i.e., $T_e \gg T_i$).

2.3. Ion sound speed

In MHD flows, the ion sound speed is the combined effect of ions and electrons, as shown in equation (5).

$$c_s = \left(\frac{\sum \gamma p}{\rho_m}\right)^{1/2} \approx \left(\frac{\gamma k_B T_e + \gamma k_B T_i}{m_i}\right)^{1/2} \tag{5}$$

In low-temperature plasmas ($T_e \gg T_i$), the ion acoustic wave velocity can be further simplified into the square root of electron temperature and ion mass.

2.4. Ion hydrodynamic wave and the phase velocity

The ion hydrodynamic wave is identified as an ion-acoustic wave in a B-field, which further extends into Alfvén waves and magnetosonic waves. The phase velocity of Alfvén waves represents the characteristic of magnetized plasma's phase velocity, where the perturbated electromagnetic wave slowly travels along the applied B-field and provides acting force to the plasma flow. On the other hand, the magnetosonic wave indicates that the wave propagates perpendicularly to the B-field. The phase velocity of Alfvén and magnetosonic waves in non-relativistic plasma are written in equations (6) and (7) [18]:

$$v_A = \frac{B}{(\mu_0 \rho_m)^{1/2}} \tag{6}$$

$$v_{ms} = (c_s^2 + v_A^2)^{1/2} \tag{7}$$

The ratio of the plasma velocity to the Alfvén velocity defines a dimensionless term known as the Alfvén Mach number.

$$M_A = \frac{v_z}{v_A} \tag{8}$$

This term gives a boundary condition to determine if plasma flow still interacts with the electromagnetic field in the MHD flow. If $M_A < 1$, the flow speed still experiences the complex effect of MHD wave and gas-dynamics effect. As soon as $M_A \geqslant 1$ is fulfilled, the MHD wave cannot act as a force to the plasma flow. Plasma flow propagation starts to be dominated purely by the steady magnetic field. Therefore, it is an essential parameter for determining plasma detachment mechanisms in MNs.

3. Model basis

Starting from the momentum equation in a steady MHD flow, shown in equation (9).

$$\rho_m (\mathbf{v} \cdot \nabla)\mathbf{v} = -\nabla \boldsymbol{p} - \frac{1}{2}\nabla^2 \boldsymbol{B} + \frac{1}{\mu_0}(\boldsymbol{B} \cdot \nabla)\boldsymbol{B} \tag{9}$$

By applying dimensional analysis, assuming that the pressure gradient and B-field gradient have the same length scale, equation (9) can be rewritten into the following forms. Detailed mathematical derivation can be found in [3]:

$$\left|\frac{\rho_m v^2}{L}\right| \cong \left|\frac{p}{L} + \frac{B^2}{2\mu_0 L} - \frac{B^2}{\mu_0 L}\right| = \left|\frac{n_p k_B T_e}{L} - \frac{B^2}{2\mu_0 L}\right| \tag{10}$$

Introducing equations (5) and (6) to equation (10) leads to a simplified equation shown in equation (11):

$$|v^2| \cong \left|c_s^2 - \frac{v_A^2}{2}\right| \tag{11}$$

This equation suggests that the final speed of acceleration processes in MN can be qualitatively determined by ion sound speed c_s and Alfvén velocity v_A. Equation (11) can be further written in a dimensionless form by dividing both sides of the equation with $v_A^2/2$ and introducing β to the equation. The microscopic characteristics, such as c_s and v_A is then implicitly hidden in the simplified momentum equation. The derivation can be found in equation (12).

$$|M_A^2| \cong \left|\frac{c_s^2}{v_A^2} - \frac{1}{2}\right| = \frac{1}{2}\left|\frac{\gamma p}{\rho_m} \Big/ \frac{B^2}{2\mu_0 \rho_m} - 1\right| = \frac{1}{2}\left|\gamma \frac{p}{p_m} - 1\right| = \frac{1}{2}|\gamma\beta - 1| \tag{12}$$

4. Result and discussion

4.1. Assessment of boundary conditions

The equation and the boundary condition show the correlation between the plasma acceleration/detachment with the plasma thermodynamic properties and magnetic pressure, implicating described in γ and β. This equation indicates that the transient from subsonic to supersonic Alfvén flow ($M_{\mathrm{A}} \equiv 1$) happened when $\beta = 3/\gamma$. For plasma in MN, it can be assumed that $\beta \approx p_e/p_{\mathrm{m}}$. The thermodynamic pressure p_e is $3/\gamma$ times larger than the magnetic pressure (note: No real solution with $M_{\mathrm{A}} = -1$; and $\gamma\beta < 0$ is invalid for actuality). Under such conditions, the contribution of the acceleration effect from the electromagnetic field is void, and plasma detachment from MN occurs. On the other extreme, the $\beta = 1/\gamma$ is expected at the $M_{\mathrm{A}} \equiv 0$ condition, which indicated flow stagnation.

Assuming $0 < \beta \ll 1/\gamma$ is sustained in the plasma, the thermodynamic pressure of plasma is much lower than its magnetic pressure according to the definition shown in equation (4), suggesting that the plasma is fully magnetized and the collisional processes are negligible. The thermodynamic pressure is preserved in the diamagnetic current by the applied B-field according to the invariant pressure theorem. $M_A \sim 0.5$ can be achieved when $\beta \sim 0$, which suggests that plasma will have trouble detaching from the strong B-field without any external perturbation. In other extreme conditions where $\beta \geqslant 3/\gamma$ sustained, plasma velocity is equal to or greater than the Alfvén velocity in MHD flow ($M_{\mathrm{A}} \geqslant 1$), suggesting plasma can no longer sense force from electromagnetic perturbation.

Based on the equations and the given assumptions, the operation range of the MN should be designed between $0 \leqslant \beta \leqslant 3/\gamma$. Suppose plasma detachment from MN appears when $\beta < 3/\gamma$, this means plasma does not fully utilize the MN for acceleration; hence, the efficiency of MN is limited. According to gas-dynamics theory, the non-fully expanded flow usually accompanies the flow discontinuity, e.g., shock wave. Resemble flow discontinuity phenomenon can also be identified in the MHD flow, such as the presence of plasma double layer or magnetic stretching, which triggers plasma detachment before $\beta = 3/\gamma$ is reached and causes non-ideal plasma expansion in MN [28].

4.2. Discussion of the β evolution along the axis of the MN

To further evaluate the evolution trend of β along the MN, β is differentiated along the flow direction z from equation (4), which leads to equation (13):

$$\frac{\partial\beta}{\partial z} = \frac{\partial}{\partial z}\left(\frac{p_e}{p_{\mathrm{m}}}\right) = \left(\frac{1}{p_{\mathrm{m}}}\frac{\partial p_e}{\partial z} - p_e\frac{\partial p_{\mathrm{m}}}{\partial z}\right)$$
$$= \frac{2\mu_0}{B^2}\left(\frac{\partial p_e}{\partial z} - \frac{p_e}{B^2}\frac{\partial B^2}{\partial z}\right)|\mathrm{v}^2| \cong \left|c_{\mathrm{s}}^2 - \frac{\mathrm{v}_{\mathrm{A}}^2}{2}\right| \tag{13}$$

Introducing the magnetic invariant characteristic (i.e., equation (3)) into equation (13) to remove the p_e from equation. Equation (14) shows a simplified correlation of $\partial\beta/\partial z$ with the magnetic flux density B and flux gradient $\partial B/\partial z$.

$$\frac{\partial\beta}{\partial z} = \frac{1}{p_{\mathrm{m}}}\left(-\frac{1}{2\mu_0} - \frac{p_e}{B^2}\right)\frac{\partial B^2}{\partial z} = \frac{1}{p_{\mathrm{m}}}\left(-\frac{1}{2\mu_0} - \frac{p_e}{B^2}\right)2B\frac{\partial B}{\partial z}$$
$$= -\frac{(p_{\mathrm{m}} + p_e)}{p_{\mathrm{m}}}\frac{2}{B}\frac{\partial B}{\partial z} = -(1+\beta)\frac{2}{B}\frac{\partial B}{\partial z} \tag{14}$$

The assessment of $\partial\beta/\partial z$ can be further separated into two directions according to the gradient of B of the MN: the convergent B-field ($\partial B/\partial z > 0$) and divergent B-field ($\partial B/\partial z < 0$), which are summarized in table 1.

For plasma at the divergent side of MN (i.e., $\partial B/\partial z < 0$), $\beta + 1 > 0$ is always valid (because $\beta > 0$ is always valid due to p_m and p_e are always positive values). On the other hand, $\partial\beta/\partial z < 0$ can never exist in the divergent MN. Vice versa, the convergent side of MN ($\partial B/\partial z > 0$) can only enable the condition of $\partial\beta/\partial \mathrm{z} < 0$.

From the above restriction, the $\beta < 1/\gamma$ better not appear in the divergent MN because the evolution of β will go through $\beta = 1/\gamma$ condition (i.e., flow stagnation condition), which indicates deceleration of plasma flow when it propagates along the z direction of divergent MN until zero velocity is reached; then plasma again get accelerated after propagate through the flow stagnation point. On the other hand, the $\beta < 1/\gamma$ also should not appear on the convergent side of MN. Otherwise, the β becomes even smaller than its initial value. Although the decreasing β still shows an acceleration to the plasma flow until a fully magnetized plasma (i.e., $\beta \approx 0$) eventually be reached. As soon as the plasma passes through the throat and reaches into divergent MN, the $\beta \ll 1/\gamma$ condition again causes an unfavorable situation at the divergent side of MN.

Table 1. Design criterium of β in MN.

$\nabla_z \beta$ condition	$\nabla_z B$ condition	β criterium	Validity
$\nabla_z \beta$ condition	$\nabla_z B$ condition	β criterium	Validity
$\partial\beta/\partial z > 0$	$\frac{\partial B}{\partial z} < 0$	$(1+\beta) > 0$	Always fulfilled
$\partial\beta/\partial z < 0$	$\frac{\partial B}{\partial z} < 0$	$(1+\beta) < 0$	Impossible
$\partial\beta/\partial z > 0$	$\frac{\partial B}{\partial z} > 0$	$(1+\beta) < 0$	Impossible
$\partial\beta/\partial z < 0$	$\frac{\partial B}{\partial z} > 0$	$(1+\beta) > 0$	Always fulfilled

Table 2. Design criterium of $\boldsymbol{p}$ and $\boldsymbol{B}$.

$\nabla_z \beta$ condition	$\nabla_z B$ condition	$\nabla_z p/\nabla_z B$ criterium
$\frac{\partial\beta}{\partial z} > 0$	$\frac{\partial B}{\partial z} < 0$	$\frac{\nabla_z p_e}{\nabla_z B} < \beta H$
$\frac{\partial\beta}{\partial z} < 0$	$\frac{\partial B}{\partial z} > 0$	$\frac{\nabla_z p_e}{\nabla_z B} > \beta H$

Either situation suggests that an overly strong B-field (where $p_e < p_m$ or $\beta < 1/\gamma$) is not constructive to the plasma acceleration through MN. To enable ideal plasma acceleration and detachment condition, $1 < \gamma\beta < 3$ should be sustained along the whole MN so that a continuous acceleration along the z-direction can be achieved by MN. This result again suggests an upper limit of applied B-field strength. The model in section 4.5 will also demonstrate the recommended upper limit of the applied B-field.

4.3. Criteria on the magnetic field gradient

Revisiting equation (13), a correlation of the plasma pressure gradient $\nabla_z p_e$ and the gradient of magnetic flux density $\nabla_z B$ can also be yielded, see the derivation shown by equation (15).

$$\frac{\partial\beta}{\partial z} = \frac{2\mu_0}{B^2}\left(\frac{\partial p_e}{\partial z} - \frac{p_e}{B^2}\frac{\partial B^2}{\partial z}\right) = \frac{1}{p_\mathrm{m}}\left(\frac{\partial p_e}{\partial z} - \frac{p_e}{p_\mathrm{m}}\frac{B}{\mu_0}\frac{\partial B}{\partial z}\right)$$
$$= \frac{1}{p_\mathrm{m}}\left(\frac{\partial p_e}{\partial z} - \beta H\frac{\partial B}{\partial z}\right) \tag{15}$$

Similar analysis performed in the previous subsection can also be applied to the discussion of $\nabla_z p_e$ and $\nabla_z B$ correlation, which is then summarized in table 2.

In expanding MN, $\nabla_z p_e/\nabla_z B$ must be smaller than a constant value βH to fulfill $\partial\beta/\partial z > 0$, while $\nabla_z p_e/\nabla_z B$ should be larger than βH at the converging side of MN, suggesting a lower applied magnetic field intensity (H) would probably be more favorable to the MN acceleration.

These criteria suggest the electron cooling effect along the z-direction of the divergent MN (i.e., $\nabla_z p_e$) must be relatively moderate than $\nabla_z B$ to fulfill the lower limit of βH. Despite the fact that higher H can provide a more relaxing criterion for the diverging degree of B-field at the expanding side of MN, the overly strong H will also demand a relatively moderate increasing gradient of B-field compared to the increase of $\nabla_z p_e$ at the convergent side of MN. This conclusion again hints that there is a threshold on the magnetic field strength when one designs an MN.

4.4. Plasma acceleration from the throat of MN

To further understand the effect of plasma acceleration, the isentropic flow equation for a de Laval nozzle is used to approximate the plasma velocity in the MN. The detailed derivation is reported in supplemental material A. A dimensionless equation describing the correlation of the thermodynamics behavior of plasma flow and its $\gamma\beta$ can derived, which is shown here in equation (16).

$$\left(\frac{T_{e,z}}{T_{e,0}}\right)^{-1} = 1 + \frac{1}{2}(\gamma - 1)\left|1 - \frac{1}{\gamma\beta(z)}\right| \tag{16}$$

The $T_{e,z}$ and $T_{e,0}$ presented in equation (16) describes the temperature of the plasma at position z and the total temperature of the plasma flow, respectively. The equation used the electron temperature to represent the internal energy of the plasma because $T_e \gg T_i$. Introducing the boundary condition, $\beta = 3/\gamma$ at $M_\mathrm{A} = 1$ (i.e., see discussion in section 4.1 and 4.2), to equation (16), one can derive a simple thermodynamic condition where

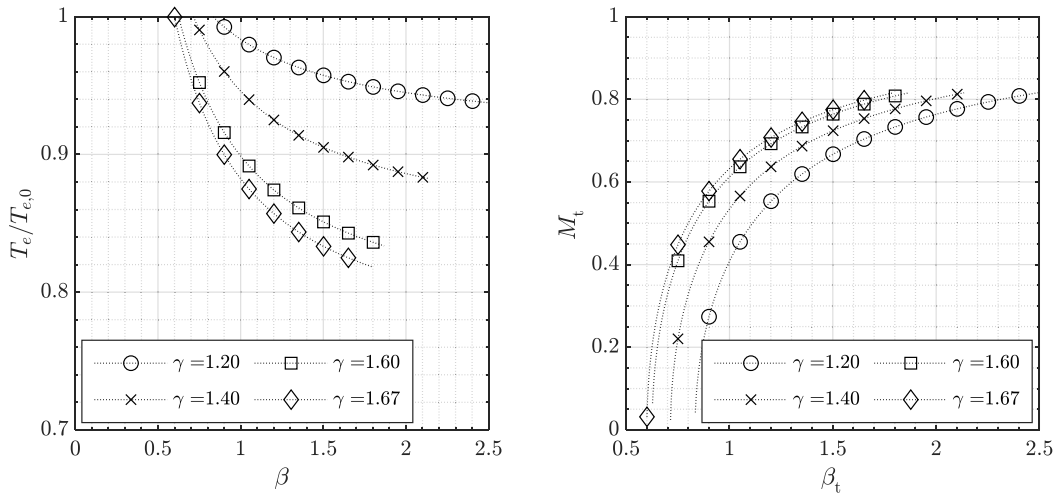

Figure 2. Correlation of temperature ratio to β at different polytropic index (γ) in MN calculated from equation (16) (left), and the Mach number at the MN throat M_t when the injected plasma flow has a different design value of β at throat of MN, i.e., β_t (right). The M_t is calculated from equation (A11).

plasma detachment occurs. The effect of β on the evolution of temperature ratio and the injected plasma Mach number of the plasma flow at the throat of MN are plotted in figure 2.

$$\frac{T_{e,M_A=1}}{T_{e,0}} = \frac{3}{\gamma + 2} \tag{17}$$

In figure 2 (left), the temperature ratio starts decaying from 1 at $\beta = 1/\gamma$ until the detachment condition ($\beta = 3/\gamma$) is reached. The figure clearly shows that more internal energy could be converted into the kinetic energy of the plasma flow when γ is closer to ideal gas condition ($\gamma = 1.67$) despite the maximum reachable β is smaller. Figure 2 (right) demonstrates the correlation of the Mach number of the injected plasma versus the β_t value (i.e., β at the throat of MN). As discussed in previous section, a non-zero plasma flow velocity is anticipated if β_t is deviated from the $1/\gamma$. The discussion of $\beta < 1/\gamma$ on the convergent side of MN is excluded since the $\beta > 1/\gamma$ must be fulfilled in the convergent MN to prevent unfavorable conditions at divergent MN (please refer to the discussion in 4.2).

In short, solely using MN cannot effectively convert the internal energy of plasma flow to the kinetic energy when plasma flow in MN is in an isothermal condition (i.e., $\gamma = 1$). Despite a perfect ideal gas condition achieved in plasma flow, equation (18) indicates that MN can only convert a limited amount of internal energy to kinetic energy even without discontinuity or external force.

4.5. Limit of magnetic flux density

Discussion in previous sections suggests the existence of an upper limit in the B-field density flux at the throat B_t. The B_t can be determined through a known total electron pressure in plasma flow $p_{e,0}$ and the designed β_t, as shown in equation (18).

$$\beta_t = \frac{p_{e,t}}{p_{m,t}} = \frac{p_{e,0}\frac{p_{e,t}}{p_{e,0}}}{B_t^2/2\mu_0} = \frac{p_{e,0}\left(\frac{T_{e,t}}{T_{e,0}}\right)^{\frac{\gamma-1}{\gamma}}}{B_t^2/2\mu_0} = \frac{p_{e,0}\quad f(\beta_t)}{B_t^2/2\mu_0} \tag{18}$$

Rearranging equation (18), the $B_t - \beta_t$ correlation is plotted in the following figure 3. The B_t required for the MN is reduced significantly when plasma has a non-zero injecting velocity at the throat of MN (i.e., $\beta_t > 1/\gamma$). which is shown in figure 3 (left) under the assumption of $p_0 = p_{0,e} = 10$Pa. On the other hand, the impact of γ to the required B_t are relatively minor. From figure 3 (right), the higher p_0 requires a stronger B_t to confine the plasma. In general, the $B_t \leqslant 250$G is sufficient to cover most of the conditions in a low-power plasma device. This threshold also aligns with the experimental result observed from a vacuum cathode arc thruster using a MN at low magnetic flux values in [12].

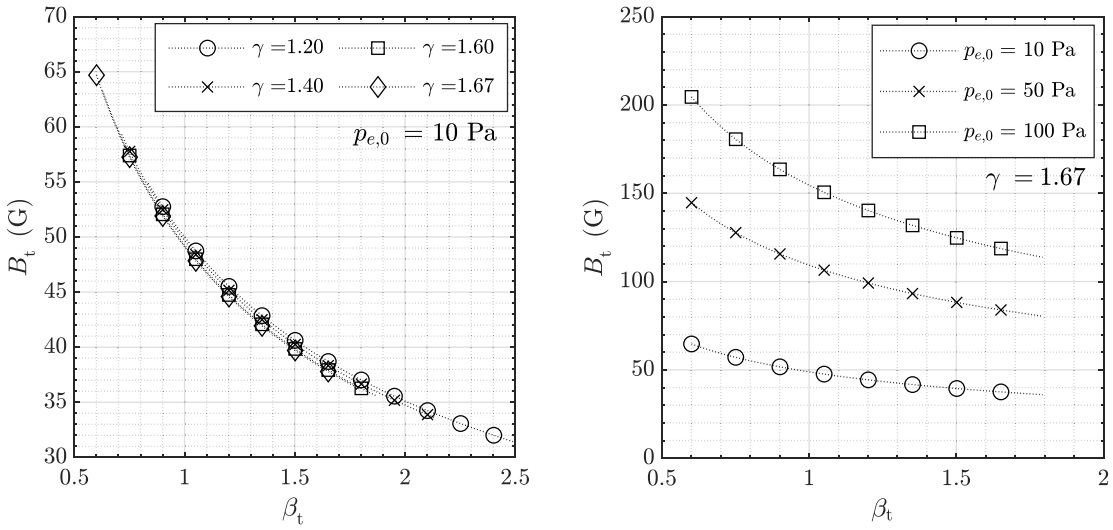

Figure 3. Evaluation of maximum magnetic flux density in different design values of β_t at throat of MN calculated from equation (18): at a fixed total pressure $p_0 = 10$Pa but with different expansion characteristics (left) and in adiabatic expansion processes but with other total pressures (right).

5. Conclusion

MN was commonly used in the neutralizer-free EP concept to provide plasma confinement and acceleration. However, these EP concepts usually suffer from low thrust efficiency. In addition, the complex MHD behavior in MN hinders the possibility of adequately designing an MN for a plasma source to convert the internal energy of plasma flow into kinetic energy. The model demonstrated in this work aims to provide an analytical assessment of the MN design and its criteria to further improve the neutralizer-free EP device's performance.

Starting from the dimensional analysis of the momentum equation of MHD flow, the discussion can be narrowed down to a few dimensionless MHD parameters, especially on the dimensionless pressure term β. The boundary condition of β derived from the dimensionless momentum equation indicates a feasible range of β for plasma acceleration in an MN located between $0 < \beta < 3/\gamma$. Further discussion on the β evolution trend in MN reveals that $\beta > 1/\gamma$ should also be fulfilled at the MN inlet to avoid plasma flow experiencing deceleration processes or anisotropic effect when propagating from MN upstream to downstream.

The discussion of β evolution trend also discloses the constraints of the electron cooling effect and the gradient of magnetic flux density on both sides of convergent-and-divergent MN, where a threshold value βH determines their ratio (Details can be found in the discussion of section 4.3).

The conversion of the plasma internal energy to the kinetic energy can be evaluated by implementing the β restriction into the isentropic flow equation of the de Laval nozzle. The assessment of the plasma flow acceleration is considered from the throat to ideal detachment condition, i.e., $M_A \equiv 1$. A dimensionless thermodynamic correlation, determined by β and γ, can be derived from the isentropic flow equation, which describes the plasma flow condition in MN.

This equation further reveals that a limited energy conversion ratio from the plasma internal energy to the kinetic energy can be achieved solely by an MN for plasma flow acceleration. As described in figure 2 (left), the energy conversion ratio $(1 - T_e/T_{e,0})$ can only reach to 19% even under ideal gas (i.e., $\gamma = 1.67$) and loss-less flow conditions. The farther the plasma deviates from the ideal gas condition, the lower the energy conversion that the MN can achieve. The limited conversion rate by solely MN suggests that the contribution of the electrostatic effect is mandatory to improve the conversion ratio further.

Additionally, the threshold of the magnetic flux density at the throat of the MN, which is usually the location of the maximum magnetic flux density of the MN, can be estimated from a known total plasma pressure at the throat. In the regular range of the total plasma pressure in a sub-kW ICP device, the magnetic flux density should not exceed 250 G to prevent an anisotropic effect in the plasma flow.

This model gives a straightforward approach to designing MN of the neutralizer-free plasma source. The result calculated from the model also demonstrates the criteria for developing an MN and a guideline to overcome the performance limitation. Last but not least, the model also suggests that the contribution from the electrostatic effect in MHD flow shall be considered to yield a higher performance in the future.

Derivation for the plasma acceleration in an MN

Assuming plasma acceleration in the divergent side of MN is an isentropic process, the correlation of the velocity at the MN throat and the final velocity at the end of MN can be written as equation (A1).

$$\mathrm{v}_\mathrm{z}^2 = \frac{2\gamma}{\gamma-1}\frac{k_\mathrm{B}T_\mathrm{z}}{m_i}\left[1-\left(\frac{T_\mathrm{z}}{T_\mathrm{t}}\right)\right]+\mathrm{v}_\mathrm{t}^2 \tag{A1}$$

Suffix t defines the condition at the MN throat, and suffix z represents the condition at z downstream from the MN throat. By dividing equation (A1) with the Alfvén velocity at z, $\mathrm{v}_{\mathrm{A,z}}^2$, the isentropic flow equation can be written as a dimensionless form led by the $M_\mathrm{A}^2(z)$ on the left-hand side of the equation. This allows the equation equation (A1) to equal the expression shown in equation (12). Considering the $T_e \gg T_i$ sustained, a new equation can be rewritten as following:

$$M_\mathrm{A}^2(\mathrm{z}) = \frac{1}{2}\,|\gamma\beta-1| = \frac{2\gamma}{\gamma-1}\frac{k_\mathrm{B}}{m_i}\frac{T_{e,\mathrm{t}}}{\mathrm{v}_{\mathrm{A,z}}^2}\left[1-\left(\frac{T_{e,\mathrm{z}}}{T_{e,\mathrm{t}}}\right)\right]+\frac{\mathrm{v}_\mathrm{t}^2}{\mathrm{v}_{\mathrm{A,z}}^2} \tag{A2}$$

Introducing equation (6) to replace v_A^2 in the right-hand side of equation (A2) can lead to equation (A3).

$$\frac{1}{2}\,|\gamma\beta(\mathrm{z})-1| = \frac{2\gamma}{\gamma-1}\frac{\rho_{m,\mathrm{z}}}{B_\mathrm{z}^2/\mu_0}\frac{k_\mathrm{B}T_{e,\mathrm{t}}}{m_i}\left[1-\left(\frac{T_{e,\mathrm{z}}}{T_{e,\mathrm{t}}}\right)\right]+\frac{\rho_{m,\mathrm{z}}\mathrm{v}_\mathrm{t}^2}{B_\mathrm{z}^2/\mu_0} \tag{A3}$$

The $\rho_{m,\mathrm{z}}$ can be written as $m_i n_{p,\mathrm{z}} + m_e n_{p,\mathrm{z}} \approx m_i n_{p,\mathrm{z}}$, assuming $n_{i,\mathrm{z}} = n_{e,\mathrm{z}} = n_{p,\mathrm{z}}$. Equation (A3) can be further rearranged as follows:

$$\frac{1}{2}\,|\gamma\beta(\mathrm{z})-1| = \frac{2\gamma}{\gamma-1}\frac{n_{p,\mathrm{t}}k_\mathrm{B}T_{e,\mathrm{t}}}{B_\mathrm{z}^2/\mu_0}\frac{n_{p,\mathrm{z}}}{n_{p,\mathrm{t}}}\left[1-\left(\frac{T_{e,\mathrm{z}}}{T_{e,\mathrm{t}}}\right)\right]+\frac{n_{p,\mathrm{t}}m_i\mathrm{v}_\mathrm{t}^2}{B_\mathrm{z}^2/\mu_0}\frac{n_{p,\mathrm{z}}}{n_{p,\mathrm{t}}} \tag{A4}$$

where the thermodynamic index γ is assumed constant along the MN. The concept of ideal gas law at the MN throat ($p_{e,\mathrm{t}} = n_{p,\mathrm{t}}\ \ k_\mathrm{B}\ \ T_{e,\mathrm{t}}$) and magnetic pressure at condition z ($p_{\mathrm{m,z}} = B_\mathrm{z}^2/2\mu_0$) are further introduced to equation (A4). In addition, the term $\frac{n_{p,\mathrm{z}}}{n_{p,\mathrm{t}}}$ can also be rewritten according to the polymetric thermodynamic correlation in isentropic flow, $\frac{n_{p,\mathrm{z}}}{n_{p,\mathrm{t}}} = \left(\frac{T_{e,\mathrm{z}}}{T_{e,\mathrm{t}}}\right)^{\frac{1}{\gamma-1}} = \chi$, where χ is used to simplified derivation. The derivation can be found in equation (A5).

$$\begin{aligned}\frac{1}{2}\,|\gamma\beta(\mathrm{z})-1| &= \frac{\gamma}{\gamma-1}\frac{p_{e,\mathrm{t}}}{p_{\mathrm{m,z}}}\left[\left(\frac{T_{e,\mathrm{z}}}{T_{e,\mathrm{t}}}\right)^{\frac{1}{\gamma-1}}-\left(\frac{T_{e,\mathrm{z}}}{T_{e,\mathrm{t}}}\right)^{\frac{\gamma}{\gamma-1}}\right]+\frac{\frac{1}{2}n_{p,\mathrm{t}}m_i\mathrm{v}_\mathrm{t}^2}{p_{\mathrm{m,z}}}\left(\frac{T_{e,\mathrm{z}}}{T_{e,\mathrm{t}}}\right)^{\frac{1}{\gamma-1}}\\ &= \frac{\gamma}{\gamma-1}\frac{p_{e,\mathrm{t}}}{p_{\mathrm{m,z}}}[\chi-\chi^\gamma]+\frac{\frac{1}{2}n_{p,\mathrm{t}}m_i\mathrm{v}_\mathrm{t}^2}{p_{\mathrm{m,z}}}\chi\end{aligned} \tag{A5}$$

Introducing $\beta(\mathrm{z}) = 1/\gamma$ as the first boundary condition (where $M_\mathrm{A} = \mathrm{v} = 0$), the velocity at the throat v_t^2 could be written as the following equation (A7):

$$-\frac{\frac{1}{2}n_{p,\mathrm{t}}m_i\mathrm{v}_\mathrm{t}^2}{p_{\mathrm{m,z}}}\chi_{\mathrm{v}=0} = \frac{\gamma}{\gamma-1}\frac{p_{e,\mathrm{t}}}{p_{\mathrm{m,z}}}[\chi_{\mathrm{v}=0}-\chi_{\mathrm{v}=0}^\gamma] \tag{A6}$$

$$\mathrm{v}_\mathrm{t}^2 = -\frac{2\gamma}{\gamma-1}\frac{k_\mathrm{B}T_{e,\mathrm{t}}}{m_i}[1-\chi_{\mathrm{v}=0}^{\gamma-1}] \tag{A7}$$

The equation (A8) shows a further derivation by inserting equation (A7) back to equation (A5).

$$\begin{aligned}\frac{1}{2}\,|\gamma\beta(\mathrm{z})-1| &= \frac{\gamma}{\gamma-1}\frac{p_{e,\mathrm{t}}}{p_{\mathrm{m,z}}}[\chi-\chi^\gamma]-\frac{\frac{1}{2}n_{p,\mathrm{t}}m_i\chi}{p_{\mathrm{m,z}}}\frac{2\gamma}{\gamma-1}\frac{k_\mathrm{B}T_{e,\mathrm{t}}}{m_i}[1-\chi_{\mathrm{v}=0}^{\gamma-1}]\\ &= \frac{\gamma}{\gamma-1}\frac{p_{e,\mathrm{t}}}{p_{\mathrm{m,z}}}[\chi-\chi^\gamma]-\frac{\gamma}{\gamma-1}\frac{p_{e,\mathrm{t}}}{p_{\mathrm{m,z}}}\chi[1-\chi_{\mathrm{v}=0}^{\gamma-1}] = \frac{\gamma}{\gamma-1}\frac{p_{e,\mathrm{z}}}{p_{\mathrm{m,z}}}\frac{p_{e,\mathrm{t}}}{p_{e,\mathrm{z}}}[\chi\chi_{\mathrm{v}=0}^{\gamma-1}-\chi^\gamma]\end{aligned} \tag{A8}$$

The term $\frac{p_{e,\mathrm{t}}}{p_{e,\mathrm{z}}} = \left(\frac{p_{e,\mathrm{z}}}{p_{e,\mathrm{t}}}\right)^{-1}$ can be written as $\chi^{-\gamma}$ by following the polymetric thermodynamic correlation in isentropic flow, while $\frac{p_{e,\mathrm{z}}}{p_{\mathrm{m,z}}}$ can be written as $\beta(\mathrm{z})$ based on equation (4). This leads to equation (A9).

$$\frac{1}{2}\,|\gamma\beta(\mathrm{z})-1| = \frac{\gamma}{\gamma-1}\beta(\mathrm{z})\chi^{-\gamma}[\chi\chi_{\mathrm{v}=0}^{\gamma-1}-\chi^\gamma]$$

$$= \frac{\gamma}{\gamma - 1}\beta(z)[\chi^{1-\gamma}\chi_{v=0}^{\gamma-1} - 1] \tag{A9}$$

The final equation can be derived by exchanging χ back to $\left(\frac{T_{e,z}}{T_{e,t}}\right)^{\frac{1}{\gamma-1}}$ and rearranging equation (A9), shown in equation (A10).

$$\chi^{1-\gamma}\chi_{v=0}^{\gamma-1} = \left(\frac{T_{e,z}}{T_{e,t}}\right)^{-1}\left(\frac{T_{e,0}}{T_{e,t}}\right) = \left(\frac{T_{e,z}}{T_{e,0}}\right)^{-1}$$
$$= 1 + \frac{1}{2}(\gamma - 1)\left|1 - \frac{1}{\gamma\beta(z)}\right| \tag{A10}$$

In addition, the Mach number at the throat of MN can also be derived by dividing both sides of equation (A7) with $c_{s,t}^2$ using equation (5), where $c_{s,t}^2 = \gamma k_B \quad T_{e,t}/m_i$ sustains considering $T_{e,t} \gg T_{i,t}$, can lead to equation (A11).

$$M_t^2 = \frac{v_t^2}{c_{s,t}^2} = -\frac{2}{\gamma - 1}[1 - \chi_{v=0}^{\gamma-1}] = \frac{2}{\gamma - 1}\left(1 - \frac{T_{e,0}}{T_{e,t}}\right) \tag{A11}$$

Data availability statement

All data that support the findings of this study are included within the article (and any supplementary files).

ORCID iDs

Yung-An Chan https://orcid.org/0000-0001-5494-0514
Georg Herdrich https://orcid.org/0000-0002-3957-762X

References

[1] Mazouffre S 2016 Electric propulsion for satellites and spacecraft: established technologies and novel approaches *Plasma Sources Sci. Technol.* **25** 033002
[2] Bathgate S N, Bilek M M M and Mckenzie D R 2017 Electrodeless plasma thrusters for spacecraft: a review *Plasma Sci. Technol.* **19** 083001
[3] Takahashi K 2019 Helicon-type radiofrequency plasma thrusters and magnetic plasma nozzles *Rev. Mod. Plasma Phys.* **3** 3
[4] Longmier B W *et al* 2014 Improved efficiency and throttling range of the VX-200 magnetoplasma thruster *J. Propuls. Power* **30** 123–32
[5] Collard T A and Jorns B A 2019 Magnetic nozzle efficiency in a low power inductive plasma source *Plasma Sources Sci. Technol.* **28** 1-18
[6] Charles C, Takahashi K and Boswell R W 2012 Axial force imparted by a conical radiofrequency magneto-plasma thruster *Appl. Phys. Lett.* **100** 113504
[7] Cannat F, Lafleur T, Jarrige J, Chabert P, Elias P-Q and Packan D 2015 Optimization of a coaxial electron cyclotron resonance plasma thruster with an analytical model *Phys. Plasmas* **22** 053503
[8] Vialis T, Jarrige J, Aanesland A and Packan D 2018 Direct thrust measurement of an electron cyclotron resonance plasma thruster *J. Propuls. Power* **34** 1323–33
[9] Peterschmitt S and Packan D 2021 Impact of the microwave coupling structure on an electron-cyclotron resonance thruster *J. Propuls. Power* **37** 806–15
[10] Boni F, Désangles V and Jarrige J 2022 Experimental characterization of thrust production mechanisms in a magnetic nozzle ECR thruster *J. Electr. Propuls.* **1** (33) 1–15
[11] Boxberger A, Behnke A and Herdrich G 2019 *Current Advances in Optimization of Operative Regimes of Steady State Applied Field MPD Thrusters 36th International Electric Propulsion Conference (Vienna, Austria, September 15-20)* IEPC-2019-585
[12] Chowdhury S and Kronhaus I 2020 Characterization of vacuum arc thruster performance in weak magnetic nozzle *Aerospace* **7** 82
[13] Takahashi K, Lafleur T, Charles C, Alexander P and Boswell R W 2011 Electron diamagnetic effect on axial force in an expanding plasma: Experiments and theory *Phys. Rev. Lett.* **107** 1–4
[14] Charles C and Boswell R W 2004 Laboratory evidence of a supersonic ion beam generated by a current-free 'helicon' double-layer *Phys. Plasmas* **11** 1706–14
[15] Meige A, Boswell R W, Charles C, Boeuf J-, Hagelaar G and Turner M M 2005 One-dimensional simulation of an ion beam generated by a current-free double-layer *IEEE Trans. Plasma Sci.* **33** 334–5
[16] Rao S and Singh N 2012 Numerical simulation of current-free double layers created in a helicon plasma device *Phys. Plasmas* **19** 093507
[17] Lieberman M A, Charles C and Boswell R W 2006 A theory for formation of a low pressure, current-free double layer *J. Phys. Appl. Phys.* **39** 3294–304
[18] Chen F 2016 *Introduction to Plasma Physics and Controlled Fusion* (Switzerland: Springer) (https://doi.org/10.1007/978-3-319-22309-4)
[19] Breizman B N, Tushentsov M R and Arefiev A V 2008 Magnetic nozzle and plasma detachment model for a steady-state flow *Phys. Plasmas* **15** 057103
[20] Takahashi K, Chiba A, Komuro A and Ando A 2016 Experimental identification of an azimuthal current in a magnetic nozzle of a radiofrequency plasma thruster *Plasma Sources Sci. Technol.* **25** 1–8055011
[21] Little J M and Choueiri E Y 2019 Electron demagnetization in a magnetically expanding plasma *Phys. Rev. Lett.* **123** 145001

[22] Moses R W, Gerwin R A and Schoenberg K F 1992 Resistive plasma detachment in nozzle based coaxial thrusters *AIP Conf. Proc.* **246** 1293–303
[23] Hooper E B 1993 Plasma detachment from a magnetic nozzle *J. Propuls. Power* **9** 757–63
[24] Ahedo E and Merino M 2012 Two-dimensional plasma expansion in a magnetic nozzle: Separation due to electron inertia *Phys. Plasmas* **19** 083501
[25] Arefiev A V and Breizman B N 2005 Magnetohydrodynamic scenario of plasma detachment in a magnetic nozzle *Phys. Plasmas* **12** 043504
[26] Winglee R, Ziemba T, Giersch L, Prager J, Carscadden J and Roberson B R 2007 Simulation and laboratory validation of magnetic nozzle effects for the high power helicon thruster *Phys. Plasmas* **14** 063501
[27] Olsen C S *et al* 2015 Investigation of plasma detachment from a magnetic nozzle in the plume of the VX-200 magnetoplasma thruster *IEEE Trans. Plasma Sci.* **43** 252–68
[28] Takahashi K and Ando A 2017 Laboratory observation of a plasma-flow-state transition from diverging to stretching a magnetic nozzle *Phys. Rev. Lett.* **118** 225002
[29] Deline C A, Bengtson R D, Breizman B N, Tushentsov M R, Jones J E, Chavers D G, Dobson C C and Schuettpelz B M 2009 Plume detachment from a magnetic nozzle *Phys. Plasmas* **16** 033502
[30] Kim J Y, Chung K-J, Takahashi K, Merino M and Ahedo E 2023 Kinetic electron cooling in magnetic nozzles: experiments and modeling *Plasma Sources Sci. Technol.* **32** 073001
[31] Sheehan J P *et al* 2014 Temperature gradients due to adiabatic plasma expansion in a magnetic nozzle *Plasma Sources Sci. Technol.* **23** 45014
[32] Zhang Y, Charles C and Boswell R 2016 Thermodynamic study on plasma expansion along a divergent magnetic field *Phys. Rev. Lett.* **116** 25001
[33] Little J M and Choueiri E Y 2016 Electron cooling in a magnetically expanding plasma *Phys. Rev. Lett.* **117** 225003
[34] Boswell R W, Takahashi K, Charles C and Kaganovich I D 2015 Non-local electron energy probability function in a plasma expanding along a magnetic nozzle *Front. Phys.* **3** 1–5
[35] Takahashi K, Charles C, Boswell R and Ando A 2018 Adiabatic expansion of electron gas in a magnetic nozzle *Phys. Rev. Lett.* **120** 45001
[36] Kim J Y, Go G, Hwang Y S and Chung K-J 2021 Dependence of the polytropic index of plasma on magnetic field *New J. Phys.* **23** 052001
[37] Vinci A E, Delavière–Delion Q and Mazouffre S 2022 Electron thermodynamics along magnetic nozzle lines in a helicon plasma *J. Electr. Propuls.* **1** 4
[38] Goedbloed J P H and Poedts S 2004 *Principles of Magnetohydrodynamics: With Applications to Laboratory and Astrophysical Plasmas* (Online: Cambridge University Press) (https://doi.org/10.1017/CBO9780511616945)